Hierarchical Pattern Recognition and Analysis Using Ellipsoidal Skeleton

Frédéric Banégas[•]
Ecole Nationale Supérieure des Mines de Saint-Etienne (ENSMSE)
Dr. François Canovas
Service de Chirurgie Orthopédique, Centre Hospitalier Universitaire Lapeyronie
Dominique Michelucci, Marc Roelens
Ecole Nationale Supérieure des Mines de Saint-Etienne (ENSMSE)
Marc Jaeger
Centre de Coopération Internationale pour la Recherche en Agronomie et le Développement (CIRAD)

Abstract :

The amount of data needed to describe both volume and surface of 3D objects is often huge and produces bottlenecks at every step of analysis. Thus, extracting relevant information in this case demands heavy and complex processing techniques. A preprocessing phase is dramatically required : data must be synthesized to accelerate analysis procedure by providing context-dependen measurements. Parameters set should not be rigid, as it can be radically different from one application to another.

The method we propose in this paper consists in transforming any digitized 3D solid – taking into account its inner points – into *Ellipsoidal Skeleton* (or E-skeleton). Based on binary shape decomposition into a union of simple sub-shapes paradigm, it also gathers relevant information about the geometry and any other set of values that seems interesting, depending on the study context. Each sub-shape and its parameters set is more generically viewed as a *feature*, which is assumed to be non-decomposable at a given *semantic level*. This semantic zoom capability for object description permits a hierarchical approach, i.e. a scale of vision control. Low semantic zoom allows crude approximation for fast pre-classification while high semantic zoom highlights finer details for precise comparison.

From this prepr ocessing stage, tasks such as object recognition and object analysis are made possible and intuitive via feature comparison. Any bottleneck is removed, ensuring fast data processing. At last, the generic structure of the E-skeleton allows not only future improvement but also practical ways to add features to the E-skeleton repertoire.

Keywords : E-skeleton, Pattern Recognition, Data Analysis, Object-to-object Distance, Feature Comparison.

[•] banegas@emse.fr, banegas@cirad.fr

1. INTRODUCTION.

Shape recognition process via decomposition is a widely investigated technique. As being rich and complex, many issues are yet to be explored. Primitives relevancy remains crucial : they should carry not only the objec geometry but also any type of information needed for analysis context. Progressive recognition wit semantic zoom may also accelerates the recognition process by early separating objects that reveals themselves too different even for a low decomposition step. Moreover, the representation method should allow generic measurements techniques for fuzzy clustering and adjustable pattern matching.

1.1. Previous Works.

Shape recognition in digital image processing covers applications ranging from robotic vision to medical imaging for tissue recognition and pathology detection. Many techniques have been investigated, based on identified principles.

Description algorithms are divided into tw classes, whether they rely on external [5][7][15]or internal expression of objects. Former ones are based on the contours (B-spline, polygons…), and latter ones use area descriptor methods (skeletons, shape decomposition). Such descriptors can be structural, like skeletons [26][28][29][30], or scalar [24][25].

Shape decomposition is a powerful technique as it achieves data reduction by imposing a particular organization on i [8][20][27]. Pixel-scaled information is organized into larger models, which provide multiscale capabilities [31] as long as the size of the clusters is variable. Some theories even suggest that such decomposition is present in human percepti [22].

The model we propose in this paper combines all aspects of internal description-based algorithms as it uses both structural – i.e. geometric – and scalar – i.e. by extracting relevant parameters in subclasses – descriptions in an hierarchical fashion thanks to semantically zoomable shape decomposition approach.

2. FROM 3D SOLID TO E-SKELETON.

We have developed the ellipsoidal skelet model [1][2] (or *E-skeleton*) to produce a shape decomposition of a 3D solid that integrates both geometry and internal parameters. Its semantic zoom capabilities provide a wide variety of representation depending on the accuracy of vision. Parameters extracted during the E-skeleton construction process can be analyzed separately or combined to compute a distance between objects as it will be discussed in Section 3.

2.1. Principle of the Ellipsoidal Skeleton.

E-skeleton computation of a 3D object is a fast pre-processing stage, taking on input a 3D point set extracted from various modalities such as CT-scan slices or MRI images. It automatically produces an analytical hierarchica representation of 3D solids, “solid” meaning that inner points are taken into account in the process.

2.1.1. Hierarchical Structure.

Geometrical substructures of the 3D solid are progressively detected (see Section 2.1.3), according to two intuitive criteria :

- a well-differentiated shape, relatively to the overall structure and the scale of vision, indicates that this substructure is a potential candidate ;
- the volume or mass of the substructure determines its rank in the detection process.

2.1.2. Decomposition According to Physical Parameters.

For any detected substructures, physical parameters are extracted via Principal Component Analysis (PCA) on the sub-cloud o

points (see Figure 1). As inner points are taken into account, features such as local centers o gravity or axis of inertia remain robust (see Section 4.1) and relevant to characterize matter dispersion [23].

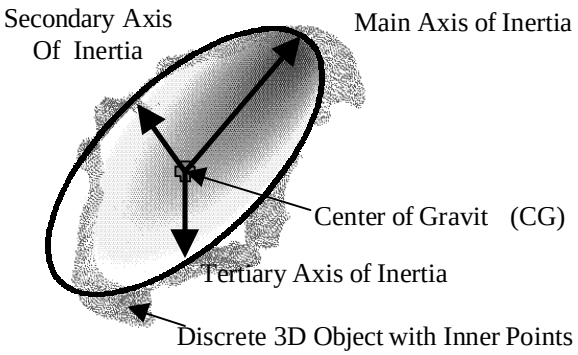

Primitive is Positioned According to Main Axis of Inertia.

Figure 1

2.1.3. Dynamic Clustering.

The first structure being the entire 3D point cloud describing the object, it is then divided into two sub-clouds. The splitting is done by using a plane orthogonal to the main axis of inertia containing the center of gravity (see Figure 2). A balancing process is performed afterward, using *dynamic clustering* (of *k-means clustering*) method [16] :

```
Repeat
    For Each existing class Ci
      Compute its Center of Gravity Gi
    EndForEach

    For Each point of the whole 3D point cloud
      Assign point to the class with closer Gi
    EndForEach
Until {G1, …, Gn-1} remains unchanged
```

The Dynamic Clustering Method, Used to Partition the 3D Point Cloud in Geometrically Relevant Subclasses.

Algorithm 1

Figure 2 illustrates Algorithm 1 :

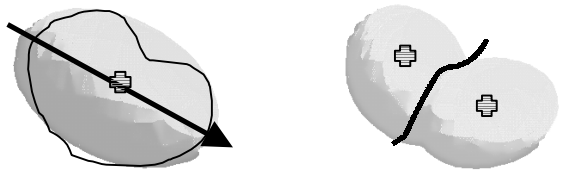

A Cloud of Points is Split in Two Parts, re-Balanced with Dynamic Clustering and New Primitives are Adjusted. Such Adjustment Ensures Steadiness an Optimal Intraclass Variance Minimization.

Figure 2

A new iteration is done, according to a *splitting criterion* that defines which sub-cloud is the best candidate. For instance, Figure 4 shows the progressive refinement of the lower part of the object, as it exhibits a more complex geometry in this area.

Strongly differentiated classes – representing substructures – are produced thanks to the dynamic clustering. The splitting criterion consists in selecting the class whose decomposition will ensure minimal intraclass variance. The intraclass variance is then optimally lowered at each new dividing step, while interclass variance is maximized, as it is stated in Equation 1 :

$$V_{total} = V_{\text{intraclass}} + V_{\text{interclass}} \qquad \text{Equation 1}$$

where V_{total} is a constant value representing the variance along the main axis of inertia of the initial point cloud.

The refining algorithm is the following :

While (V_{intra} > $V_{threshold}$) Or (*#classes* < *#threshold*)
  For Each existing class C_i
    Computation of inertia matrix of C_i
    Computation of intraclass variance V_i of C_i
    Rough Splitting of C_i into C'_i and C''_i
    "Fake" Dynamic Clustering on all classes
    Computation of intraclass variances V'_i and V''_i
  EndForEach
  Effective Split of class with smallest $\frac{V'_i+V''_i}{V_i}$
  Effective Dynamic Clustering on all classes
  Computation of ne V_{intra}
EndWhile

Algorithm 2

where $\frac{V'_i+V''_i}{V_i}$ is the splitting criterion.

2.1.4. Semantic Zoom.

Each hierarchical level is defined by the number of primitives used to represent the object This number is incremented at each new detection, producing a *semantic level*.

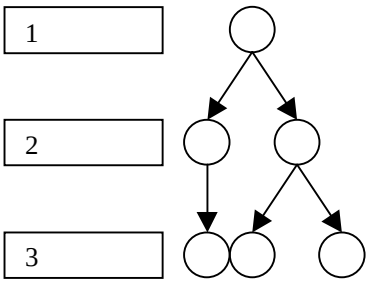

Hierarchical Tree : Semantic Levels Stored Historically during the Automatic Decomposition Process.

Figure 3

Both hierarchical and analytical [9] nature of this tree allow the selection of a representation according to the preferred accuracy.

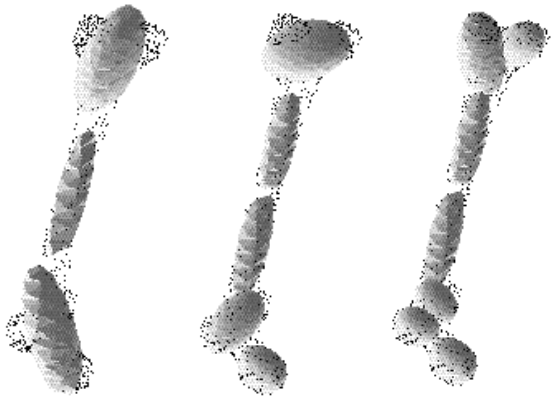

Three *Semantic Levels* (SL) of a *femur* produced by E-skeleton.

Figure 4

2.2. Feature Extraction.

Features can be integrated as externa functions (see Secti 3.1). A feature is represented by a couple of functions *(g ; f_d)* where :

- *g* is the *extraction function* for the given parameter, e.g. inertia matrix computation, mean density calculation …etc. Argument for *g* is the raw subclass point cloud.
- f_d is the *distance function* associated with the parameter (see Equation 4), e.g. euclidean distance for 3D coordinates, difference for means density …etc.

3. ANALYSIS AND RECOGNITION VIA E-SKELETON.

Once computed, the E-skeleton is ready for comparison, analysis and pattern matching purposes. A mathematical framework for E-skeleton has been developed to ensure flexibility.

3.1. Formal Definition of the E-Skeleton.

For a given semantic level *n*, each 3D objec is defined via the following vector :

$((\alpha_1^1,...,\alpha_p^1),...,(\alpha_1^{n-1},...,\alpha_p^{n-1}))$	Equation 1

where $(\alpha_1^i,...\alpha_p^i)$ is the set of parameters attached to primitive E_i ($i \in \{1,..n-1\}$). Each elemen α_j^i is a vector of R^k, depending on the parameter dimension. For instance, the mean density is a 1-dimension parameter while orientation is a 3-dimension parameter in 3D space, as it contains the three *Euler's angle* values.

To perform measurements between E-skeletons, users must choose a subset of parameters for each primitive E_i. Once it has been done, data is ready to be analyzed through the *Measurement Pipeline*.

3.2. The Measurement Pipeline.

For *m* 3D solids to be compared at a given semantic level, the measurement pipeline is organized as follows :

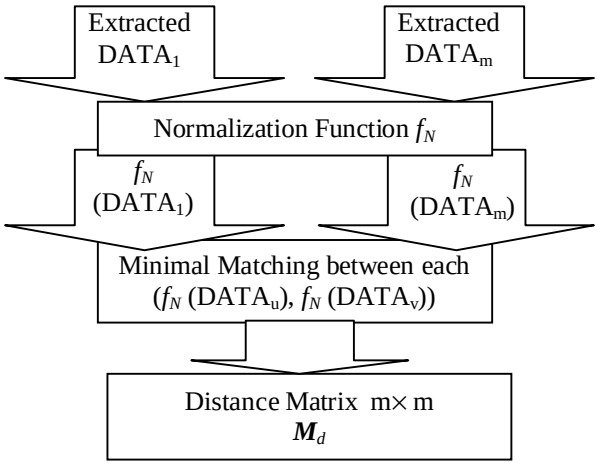

The Measurement Pipeline : Extracted Parameters are Normalized and Optimally Matched. A Distance Matrix is Produced on Output.

Figure 5

Selected parameters are normalized before entering into the effective computation process (see Section3.2.1). A best matching stage (Section 3.2.2) is then performed between each subclass of every object introduced into the pipeline. The difference values are combined into one, which we call *object-to-object distance* (see Section 3.2.3).

3.2.1. The Normalization Functio f_N.

For specific needs, any arbitrary normalization function can be integrated into the pipeline. All input data will be mapped through this function before being used. Each parameter can be weighted, or ranged between [0 ; 1] for instance. Identity function is also useful for comparison purposes (see Section 3.3).

3.2.2. Best Matching Process.

For objects O_1 and O_2 at semantic level *n*, defined respectively by the following vectors :

$$v_1 = ((\alpha_1^1,...,\alpha_q^1),...,(\alpha_1^{n-1},...,\alpha_q^{n-1}))$$
$$v_2 = ((\beta_1^1,...,\beta_q^1),...,(\beta_1^{n-1},...,\beta_q^{n-1})) \quad \text{Equation 2}$$

where $q \le p$, we cal *distance between O_1 and O_2*, the functi $d(v_1,v_2)$ defined as follows :

$$d(v_1,v_2) = \min_{(l,l' \in \{1,...,n-1\})} \sum_{l,l'} \delta((\alpha_1^l,...,\alpha_q^l),(\beta_1^{l'},...,\beta_q^{l'}))$$

Equation 3

where :

$$\delta((\alpha_1^l,...,\alpha_q^l),(\beta_1^{l'},...,\beta_q^{l'})) = f_{d1}(\alpha_1^l,\beta_1^{l'}) + ... + f_{dq}(\alpha_q^l,\beta_q^{l'}) \quad \text{Equation 4}$$

$f_{d1...l}$ being any distance function matching the type of parameters in argument (euclidean distance for points, difference for densities …etc.)(see Section 2.2).

$d(v_1,v_2)$ in Equation 3 is found using a classical *minimal cost maximum flow* technique in order to avoid the computation of *O(n!)* values. The input graph is produced by linking every $(\alpha_1^i,..\alpha_q^i)$ from objec O_1 to every $(\beta_1^i,...\beta_q^i)$ and valuating each link with appropriate function $f_{d1..q}$ shown in Equation 4. This method is a particular case of a more generic method for calculating distances between graphs [19][18].

3.2.3. The Distance Matrix M_d.

On output $\boldsymbol{M_d}$ contains all distances between the *m* input objects. It is an *m*×*m* symmetrical

matrix, whose diagonal is set to zero, as $d(v,v) = 0$ for any v.

3.3. Object Comparison.

Object comparison is based on *feature comparison* : the user selects the relevant features for the measurement, and possibly an normalization function. Any new feature can be created and integrated into the E-skeleton repertoire using rules described in Section 2.2.

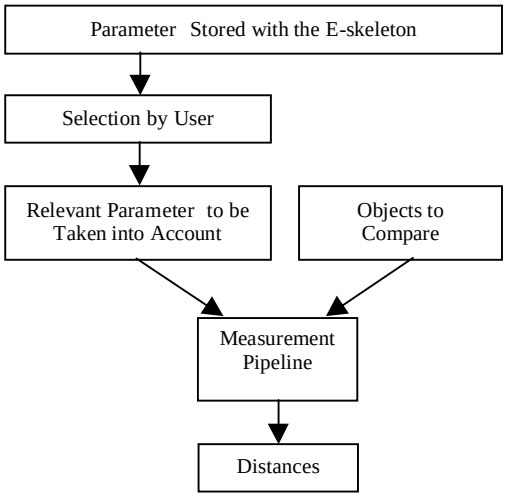

To Compare Objects, User must Select Relevant Parameters to be Measured. The Output Distance Matrix allows Overview of Objects for Analysis and Clustering Capabilities.

Figure 6

Distances can have an objective meaning (for instance volume difference or angle measured between two sub-shapes), but are rather designed for classification purposes.

3.4. Object Recognition.

Distance between objects are useful to classify them afterward. Once a scale of vision (i.e. the number of classes) and parameters have been set, the distance matrix can provide pattern recognition capabilities.

To enhance and accelerate the recognition process, *progressive vision* can be used. It basically consists in comparing E-skeletons at low number of classes and progressively refine them while classifying the objects at the same time. Using this method avoids mistakes in the clustering resulting from too detailed E-skeletons, and allows rapid differentiation even at early stages of comparisons.

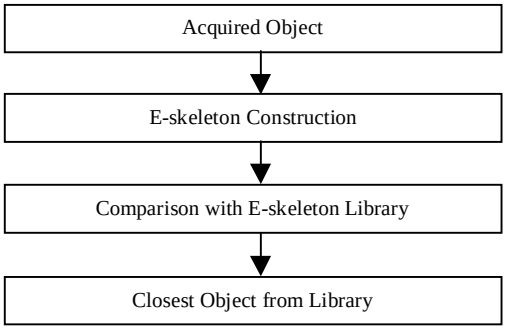

Unknown Objects Can Be Recognized Using an E-skeleton Library.

Figure 7

4. RESULTS AND APPLICATIONS.

Robustness tests and applications of the E-skeleton are presented in this section.

4.1. E-skeleton Robustness.

For feature analysis and template matching, the model has to fulfill the following goals :

- noise resistance, that is to discretization error (especially for anisotropic spatia resolution of the digitizing device) and segmentation error (from the expert) ;
- viewpoint invariance ;
- subsampling-proof, in order to be independent from digitization resolution.

Efforts have been made on robustness experimentation. A large set of 3D solids have been used, from medical data. The following test sets we used are :

- the ***carpal bones set*** : five CT-scan exams of the same patient, taken in various positions (rotation and translation). Each exam exhibits eight different bones (carpal bones) separately segmented by an expert ;
- the ***tooth set*** : a CT-scan exam of whole lower and upper jaws. All teeth have been

segmented and identified by an expert Comparisons can be performed between hemi-arcade of the same jaw due to symetry ;

- the ***femur set*** : a CT-scan exam of the right and left femur of a patient, automatically segmented from density threshold using *Corpus 2000* (see Section 4.3).

We have measured the classes variation for increasing number of classes. For this purpose, we define the following indicators :

$\bar{\varepsilon}_{CoG}$ is the average variation of the center o gravity distance from the global center of gravity of each object, for all classes relatively to reference exam. For each bone, the maximum variation is taken among the classes available, and a mean value is calculated over the five exams.

$\bar{\varepsilon}_{inertia}$ is the average variation, for all classes, of the *X*, *Y* and *Z* coordinates of the three vectors of inertia, measured between an object and the corresponding one in the reference exam. For each bone, the maximum variation is taken among the classes available, and a mean value is calculated over the five exams. The used referential is the proper one for each object, i.e. the set of the three main axis of inertia using the one-primitive decomposition.

The first indicator measures the average class position variation, the second indicator exhibits the clustering variation as the object is translated and rotated in space.

4.1.1. Noise and Error Resistance.

For this test, we have used the *carpal bones set*, as it combines segmentation error from the expert and strong sampling variation as the scanner is subject to anisotropy along the *Z* axis. Ratio between the *XY* resolution and *XZ* or *YZ* resolution is 3.22 mm in our case, which affects the object shape as it is rotated throughout the five exams.

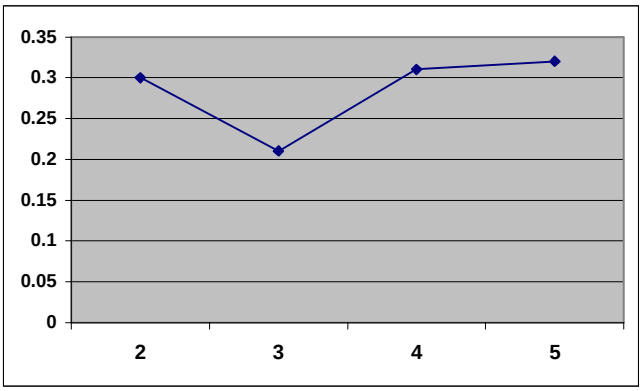

$\bar{\varepsilon}_{CoG}$ from Global Center of Gravity (in mm) according to the Number of Classes. Example for *hamatum*. *XY* to *XZ* resolution ratio is 3,22.

Figure 8

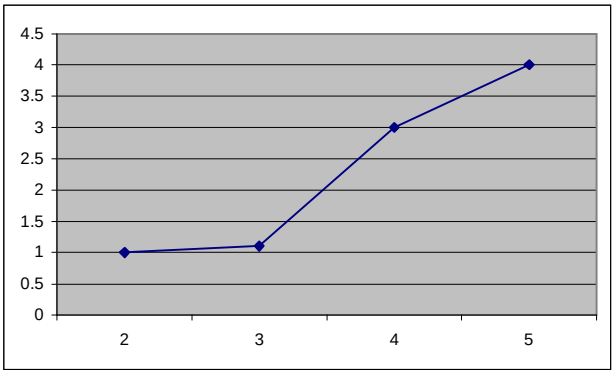

$\bar{\varepsilon}_{inertia}$ (in mm) according to the Number of Classes. Example for *hamatum*. *XY* to *XZ* resolution ratio is 3,22.

Figure 9

We have also measured the average value o $\bar{\varepsilon}_{CoG}$ and $\bar{\varepsilon}_{inertia}$ throughout all exams and bones, which gives us a variation measured among 40 objects :

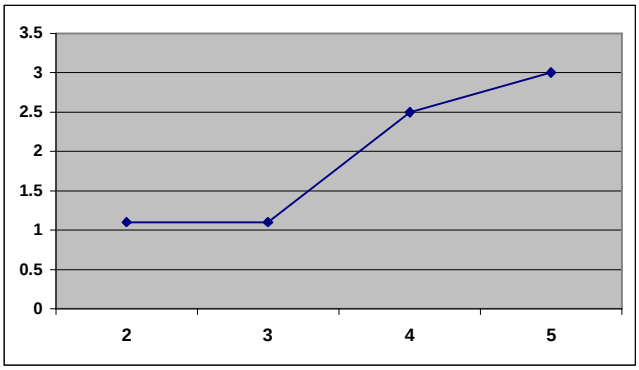

Average Inertia Vector Coordinates Variation (in mm) according to the Number of Classes. Average Value for *all bones*. *XY* to *XZ* resolution ratio is 3,22.

Figure 10

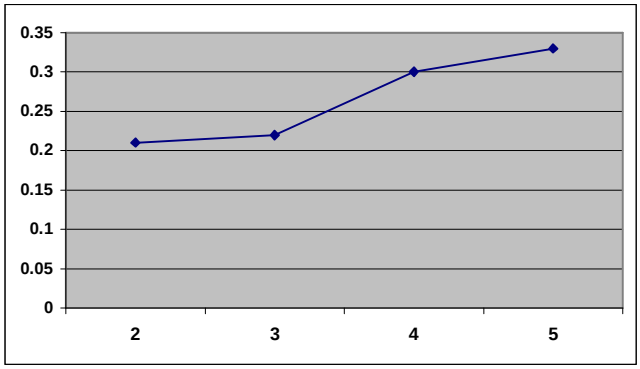

Average Center of Gravity Position Variation from Global Center of Gravity (in mm) according to the Number of Classes. Average Value for *all bones*. *XY* to *XZ* resolution ratio is 3,22.

Figure 11

If we suppress the anisotropy along *Z* axis (by modifying the *z* coordinate value of each point so that *XY* to *XZ* ratio becomes 1,0), $\bar{\varepsilon}_{CoG}$ and $\bar{\varepsilon}_{inertia}$ have no significant variation (i.e. << 1,0 mm) until a high number of classes is reached. This behavior exhibits strong resistance to surface error, as object boundaries in CT-scan exams are not clearly defined, even for high density tissues.

4.1.2. Viewpoint Invariance.

For this purpose, we have artificially rotated objects of all sets described in Section 4.1 and suppressed the *Z* anisotropy so that sampling frequency remains unchanged. E-skeleton shown no significant variation, even for a great number of classes (about 15, which is actually never reached for comparison or recognition purposes).

This behavior is normal, as E-skeleton algorithm does not rely on the processing order of points, and that inertia matrix remains invariant to rotation and translation.

4.1.3. Subsampling Robustness.

For this test, we have progressively lowered the number of points of each object, and performed measurements using the *carpal bones set*. The following table summarizes the results we obtained :

0.02	0.01	0.004	0.002	0.001	**2**
1.2	0.41	0.32	0.1	0.04	**3**
2.22	0.85	0.72	0.62	0.25	**4**
3.25	2.8	2.5	2.32	1.0	**5**
1:20 1938 pts	**1:15 2584 pts**	**1:10 3876 pts**	**1:5 7753**	**1:2 19383**	**#classes**

Distance Values Using both Center of Gravity Coordinates and Vectors of Inertia Coordinates. Subsampling Exhibited no Recognition Issue in the Bones Classification on this set.

Table 1

Greater distance is obtained from 1:20 subsampling, but this variation was not sufficient to introduce errors in the classification made in Section 4.2.

4.2. Object Recognition.

The following tests were performed on the sets described in Section 4.1 :

- classifying all bones in the *carpal bones set* ;
- showing that the two distinct femurs in the *femur set* are the same (we suppressed the symmetry by only using absolut values) ;
- matching each tooth in the *tooth set* with the corresponding tooth in the appropriate hemi-arcade.

0	8	3	3	3	67	65	64	63	65	54	53	52	53	53
8	0	8	7	7	69	67	66	66	67	54	53	52	54	53
3	8	0	4	4	67	65	64	63	65	53	52	52	52	52
3	7	4	0	1	68	66	65	64	66	53	53	51	53	53
3	7	4	1	0	68	66	65	65	66	53	53	52	53	53
67	69	67	68	68	0	4	5	6	3	68	66	68	68	66
65	67	65	66	66	4	0	6	7	3	66	64	65	65	64
64	66	64	65	65	5	6	0	3	5	68	66	68	67	66
63	66	63	64	65	6	7	3	0	6	67	65	66	66	65
65	67	65	66	66	3	3	5	6	0	67	65	66	66	65
54	54	53	53	53	68	66	68	67	67	0	5	2	3	4
53	53	52	53	53	66	64	66	65	65	5	0	4	3	1
52	52	52	51	52	68	65	68	66	66	2	4	0	2	3
53	54	52	53	53	68	65	67	66	66	3	3	2	0	2
53	53	52	53	53	66	64	66	65	65	4	1	3	2	0

Clustering of the *hamatum*, *capitatum* an *lunatum* (5 exams) Resulting from Distance Measurement between Objects in the *carpal bones set*. 3 Classes per Object are Used, and Distance Combines the Position and the Shape of Each Classes.

Table 2

Table 2 shows only a portion of the entire distance matrix (see Section 3.2.3). Clustering has been made successfully using three classes per object. Less classes does not allow a precise differentiation of objects. More classes are useless or can exhibit finer details of object, resulting in a too precise clustering. Low values indicates distances between corresponding bones throughout the five exams (gray background).

For the *femur set*, we verified that left and right femur were detected as the same object even for a great number of classes. The symmetry can then be determined by using a common referential for the two objects.

	11	21	31	41	15	25	35	45
11	0.	20.1	27.4	27.1	34.9	33.3	26.5	29.4
21	20.1	0.	29.5	30.3	38.6	35.4	24.4	27.6
31	27.4	29.5	0.	3.7	18.9	19.4	28.7	26.
41	27.1	30.3	3.7	0.	18.6	18.7	28.2	26.7
15	34.9	38.6	18.9	18.6	0.	4.4	41.6	40.4
25	33.3	35.4	19.4	18.7	4.4	0.	39.3	36.9
35	26.5	24.4	28.7	28.2	41.6	39.3	0.	8.9
45	29.4	27.6	26.	26.7	40.4	36.9	8.9	0.

Clustering of Teeth 1 and 5 Over the Four Hemi-Arcades. Each Tooth has Only One "Twin", as Jaws are Only Symmetrical Relatively to the Sagittal Plane.

Table 3

Note that in Table 3, teeth 11 and 21 seem to be very distant from one to another (distance value is 20.1). It is because tooth 21 exhibits a pathological anatomy in this exam.

For molars, clustering was not so precise as the shapes are not well-differentiated. Better results were obtained using *progressive vision method* (see Section 3.4).

4.3. The Analysis Editor

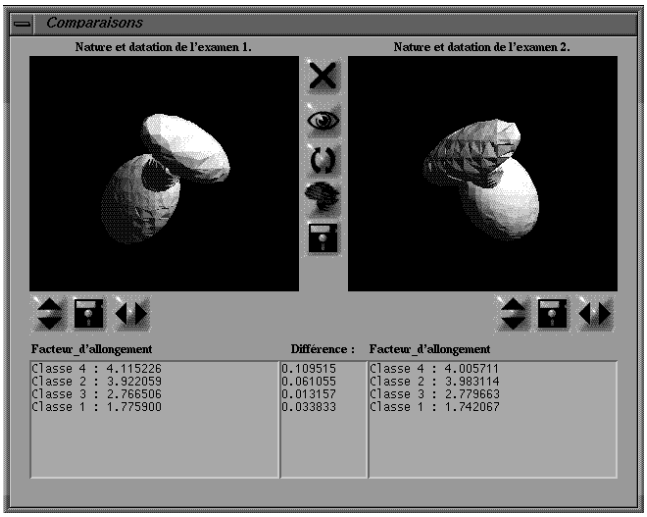

Work on the *femur set.* Parameters (Elongation Factor Here) Can Be Interactively Chosen and Computed on a Collection of Arbitrary Objects Transformed into E-skeletons.

Figure 12

Measuring parameters on E-skeletons allows quick and precise study of rigid bodies. We have developed a plug-in for the *CIRAD* software *Corpus 2000* to interactively choose the desired parameters. The data is then calculated on the selected objects, and distance matrix is produced for classification purposes.

This tool was used for a study on carpal bones growth for children [17] made by Dr. Françoi Canovas *et al.* (Orthopedic Surgery Service, Lapeyronie Hospital, Montpellier, France) : using E-skeletons, new data could be extracted and correlated with both skeletal and chronological ages. A medical follow-up was set up for growth monitoring on a population of 25 children.

5. CONCLUSION AND FUTURE WORK.

We have presented a new generic model for pattern recognition and analysis. It allows feature comparison via parameters selection, and interactive study of 3D objects.

Distance values often lack of intuitive sense and should not be used "as is", unless specific

features are intentionally chosen. They should be used only relatively to other distance values for classification purposes (including fuzzy classification). While being sometimes difficult to understand, they have proven to be efficient and robust for pattern matching.

We are now working on three directions :

- geometric primitives are classic superquadrics [7], i.e. ranging from cuboids to cylinders, including spheres and ellipsoids. These shapes parameters are being integrated to the feature list. I seems interesting to extend the primitive repertoire in order to enhance characterization capabilities of the E-skeleton [21] ;
- "close" primitives in terms of feature should be regrouped (e.g. two cylinder-shaped classes having the same orientation can be seen as a single tube) ;
- explore new features to enhance classification capabilities and study how to create "intuitive" distance values.

E-skeleton has been integrated in the CIRAD medical imaging software *Corpus 2000*, available on SGI (IRIX), HP (HPUX) and PC (win95, 98, NT) platforms.

Bibliography

[1] F. Banégas, D. Michelucci, M. Roelens and M. Jaeger, "*Automatic Extraction of Significant Features from 3D Point Clouds by Ellipsoidal Skeleton. Applications in Vision and Geometrical Characterization.*", International Conference on Visual Computing '99, Proceedings of IFIP TC5/WG5.10 and CSI, pp. 58-67.

[2] F. Banégas, D. Michelucci, M. Roelens, M. Jaeger and Dr. F. Canovas, "*Hierarchical Automated Clustering of Cloud Point Set by Ellipsoidal Skeleton. Application to Organ Geometric Modelling from CT-scan Images.*", SPIE's International Symposium on Medical Imaging 1999, Poster Session 3661-128, SPIE Proceedings on Poster Sessions.

[3] D. Attali, P. Bertolino, A. Montanvert, "*Using Polyballs to Approximate Shapes and Skeletons.*", 1994.

[4] A. Barr, "*Global and Local Deformations of Solid Primitives.*", Computer Graphics, volume 18, pp. 21-30, ACM Press, 1984.

[5] J.D. Boissonnat, "*Geometric Structures for Three-Dimensional Shape Representation.*", ACM Trans. on Graphics, volume 3, 266-286, ACM Press, 1984.

[6] V. Burdin, C. Roux, C. Lefèvre, E. Stindel, "*Modeling and Analysis of 3d Elongated Shapes with Applications to Long Bone Morphometry. ",* IEEE Transactions on Medical Imaging, volume 15, pp. 79-91, IEEE, February 1996.

[7] A. Leonardis, A. Jaklic, F. Solina, "*Superquadrics for Segmenting and Modeling Range Data. ",* IEEE PAMI, Volume 19, pp. 1289-1295, IEEE, November 1997.

[8] S. Muraki, "*Volumetric Shape Description of Range Data Using Blobby Model.*", Computer Graphics, volume 25, pp.227-235, ACM Press, 1991.

[9] A. Pasko, V. Adzhiev, A. Sourin, V. Savchenko, "*Function Representation in Geometric Modeling : Concepts, Implementation and Applications. ",* Visual Computer, pp. 429-446, Springer-Verlag Eds., 1995.

[10] M. L. Rhodes, "*Computer Graphics and Medicine : A Complex Partnership.*", IEEE Computer Graphics And Applications, pp. 22-28, IEEE, January-February 1997.

[11] V. V. Savchenko, A. A. Pasko, O. G. Okunev, T. L. Kunii, "*Function Representation of Solids Reconstructed from Scattered Surface Points and Contours.*", Eurographics'95, Blackwell Publishers, 1995.

[12] R. Durikovic, K. Kaneda, H. Yamashita, "*Reconstructing a 3d Structure with Multiple Deformable Solid Primitives. ",* Computer & Graphics, Volume 21, pp. 611-622, Pergamon, 1997.

[13] E. Bittar, N. Tsingos, M. P. Gascuel, "*Automatic Reconstrucion of Unstructured 3D Data : Combining a Medial Axis and Implicit Surfaces. ",* Eurographics'95, Volume 14, F. Post and M. Gobel eds., 1995.

[14] D. Silver, N. J. Zabusky, "*Quantifying Visualization for Reduced Modeling in Nonlinear Science : Extracting Structures from Data Sets ",* The Journal

of Visual Communications and Image Representation, Volume 4, pp. 46-61, 1993.

[15] B. Soroka, R. Andersson, R. Bajcsy, "*Generalized Cylinders from Local Aggregation of Sections. "*, Pattern Recognition, Volume 13, 1981.

[16] E. Diday, "*Une Nouvelle Méthode en Classification Automatique et Reconnaissance de Formes : la Méthode des Nuées Dynamiques.*", Rev. Statist. Appl., volume 19, pp. 19-33, 1971.

[17] F. Canovas, F. Banégas, C. Cyteval, M. Jaeger, A. Dimeglio, C. Sultan, F. Bonnel, " *Carpal Bone Maturation Assessment by Image Analysis from CT-scans.*", to be published in.

[18] P. Ferraro, C. Godin, "*An Algorithm for Comparing Unordered Tree Graphs Based on a Minimum Cost Mapping with a Minimal Connectivity.*", Third International Conference on Orders, Algorithms and Applications, August 25-27 1999, Montpellier, France.

[19] K. Zhang, "*A Constrained Edit Distance Between Unordered Labeled Trees.*", Algorithmica (1996), vol. 15, pp. 205-222, 1996.

[20] I. Pitas, A. N. Anastasios, " *Morphological Shape Decomposition.*", IEEE PAMI, vol. 12, No. 1, pp. 38-45, 1991.

[21] J. Martin, A. Pentland, S. Sclaroff, R. Kikinis, "*Characterization of Neuropathological Shape Deformation..*", IEEE PAMI, vol. 20, No. 2, pp. 97-112, February 1998.

[22] I. Biederman, "*Recognition-by-components : a Theory of Image Human Understanding. "*, Psychological Review, 94, pp. 115-147, 1987.

[23] M. R. Spiegel, "*Théorie et Application de la Mécanique Générale*.", Mc Graw Hill, 1983.

[24] S. Sclaroff, A. Pentland, "*Modal Matching for Correspondence and Recognition.. "*, IEEE PAMI, June 1995.

[25] E. P. Simoncelli, " *A Rotation Invariant Pattern Signature.*", Proceedings of Third IEEE International Conference on Image Processing, vol. III, pp. 185-188, Lausanne, Switzerland, 16-19 September 1996.

[26] E. Ferley, M.P Gascuel, D. Attali, "*Skeletal Reconstruction of Branching Shapes.*", Implicit Surfaces '96 : 2nd International Workshop on Implicit Surface, Eindhoven, The Netherlands, October 1996.

[27] J.L. Mari, J. Sequeira, C. Guiard, "*Caractérisation de Volumes Numériques Binaires par Surfaces Implicites.*", Proceedings of 12èmes Journées de l'AFIG'99, Reims, France, 24-26 November 1999.

[28] M. Näf, O. Kübler, R. Kikinis, M.E. Shenton and G. Székely, " *Characterization and Recognition of 3D Organ Shape in Medical Image Analysis Using Skeletonization.*", IEEE Workshop on Mathematical Methods in Biomedical Image Analysis, San Francisco, USA, June 20, 1996.

[29] D. Attali, A. Montanvert, *"Semicontinuous Skeletons of 2D and 3D Shapes.*", Proceedings of Second International Workshop on Visual Form, pp. 32-41, World Scientific, 1994.

[30] Lee D.T., "*Medial Axis Transformation of a Planar Shape.*", IEEE PAMI, 4(4) :363-369, 1982.

[31] B.S. Morse, S.M. Pizer and C.A. Burbeck, " *General Shape and Specific Detail : Context-Dependent Use of Scale in Determining Visual Form.*", Proceeding of the Second International Workshop on Visual Form, pp. 374-383, World Scientific, 1994.